https://doi.org/10.5194/egusphere-2023-2932
Preprint. Discussion started: 26 February 2024

A rapid application emissions-to-impacts tool for scenario assessment: Probabilistic Regional Impacts from Model patterns and Emissions (PRIME)

Camilla Mathison[1,3], Eleanor J. Burke[1], Eszter Kovacs[3], Gregory Munday[1], Chris Huntingford[2], Chris D. Jones[1,7], Chris J Smith[3,4], Norman J. Steinert[5], Andy J Wiltshire[1,6], Laila K. Gohar[1], and Rebecca M. Varney[6]

[1]Met Office Hadley Centre, Exeter, UK
[2]UK Centre for Ecology and Hydrology, Wallingford, UK
[3]University of Leeds, Leeds, UK
[4]International Institute for Applied Systems Analysis (IIASA), Laxenburg, Austria
[5]NORCE Norwegian Research Centre, Bjerknes Centre for Climate Research, Bergen, Norway
[6]Faculty of Environment, Science and Economy, University of Exeter, Exeter, UK
[7]School of Geographical Sciences, University of Bristol, Bristol, UK

Correspondence: Camilla Mathison (camilla.mathison@metoffice.gov.uk)

Abstract.

Climate policies evolve quickly and new scenarios designed around these policies are used to illustrate how they impact global mean temperatures using simple climate models (or climate emulators). Simple climate models are extremely efficient although limited to showing only the global picture. Within the Intergovernmental Panel on Climate Change (IPCC) framework, there is a need to understand the regional impacts of scenarios that include the most recent science and policy decisions quickly to support government in negotiations. To address this, we present PRIME (Probabilistic Regional Impacts from Model patterns and Emissions), a new flexible probabilistic framework which aims to provide an efficient means to run new scenarios without the significant overheads of larger more complex Earth system models (ESMs). PRIME provides the capability to include the most recent models, science and scenarios to run ensemble simulations on multi-centennial timescales and include analysis of many variables that are relevant and important for impacts assessments. We use a simple climate model to provide the global temperatures to scale the patterns from a large number of the CMIP6 ESMs. These provide the inputs to a weather generator and a land-surface model, which generates an estimate of the land-surface impacts from the emissions scenarios. Here we test PRIME using known scenarios in the form of the Shared Socioeconomic Pathways (SSPs) to demonstrate that PRIME reproduces the climate response to a range of emissions scenarios, as shown in the IPCC reports. We show results for a range of scenarios including the SSP5-8.5 high emissions scenario, which was used to define the patterns; SSP1-2.6, a mitigation scenario with low emissions and SSP5-3.4-OS, an overshoot scenario. PRIME correctly represents the climate response for these known scenarios, which gives us confidence that PRIME will be useful for rapidly providing probabilistic spatially resolved information for novel climate scenarios; substantially reducing the time between the scenarios being released and being used in impacts assessments.

https://doi.org/10.5194/egusphere-2023-2932
Preprint. Discussion started: 26 February 2024

1 Introduction

A major gap currently exists in our capability to rapidly assess and predict regional impacts of climate change in response to novel future pathways of climate change and rapidly evolving policies. Detailed climate impacts models exist that assess the regional implications of future climate scenarios for a range of impacts sectors, such as: crops, biomes, water, fire and permafrost, for example through the Inter-Sectoral Impacts Model Intercomparison Project (ISIMIP; Frieler et al., 2017; Warszawski et al., 2014, 2013). ISIMIP provides a consistent framework for assessing climate impacts using a large ensemble of models across a range of sectors. However, impact models are often specific to particular sectors and are in themselves complicated to set up. Usually, their use occurs at the end of a long chain of events: commencing with generation of emissions scenarios, running one or more Earth system models (ESMs), potentially bias-correcting ESM output, then finally running the impact model.

In order to assess impacts resulting from climate change more systematically, ISIMIP provides output of ESMs to impact modellers. But even then, there is a long delay from creation of the scenarios to our ability to assess their impacts. For example, the most recent impacts assessment of the Intergovernmental Panel on Climate Change (IPCC), the Sixth Assessment Report (AR6) Working Group II (Climate Change Impacts, Adaptation and Vulnerability: WGII) (Pörtner et al., 2022), relies heavily on literature based on impacts studies using output from the previous generation of the Coupled Model Intercomparison Project (CMIP5), rather than the most recent CMIP6 used in AR6 Working Group I (IPCC, 2021). This means that both the scenarios (RCPs; van Vuuren et al., 2011) and climate models themselves (e.g., HadGEM2-ES Jones et al., 2011; Collins et al., 2011) used to assess climate impacts by the IPCC are at least a decade old.

This apparent bottleneck is caused by the significant issue that ESMs, which are the main mechanism for projecting future climate change, are computationally demanding, so only a limited number of simulations may be performed. As ESMs take years to develop, test, and run, scenarios of future climate change are only produced periodically on a timeframe designed to align with IPCC assessment reports, such as contributions to the CMIP phases (Taylor et al., 2012; Eyring et al., 2016). Nevertheless, ESMs remain the best tools for understanding mechanisms of climate change, and regional climate projections could not be performed without them.

One popular method to enable projections of future climate change for novel emissions scenarios, and yet captures the process understanding implicit in the ESMs simulations that do exist, is via "pattern-scaling" (Zelazowski et al., 2018; Huntingford et al., 2010). Such scaling assumes that local and monthly changes in near-surface meteorological conditions correlate linearly with the level of global warming. Lee et al. (2021) note that pattern scaling has known limitations, for example having lower skill for variables with large spatial variability (Herger et al., 2015; Tebaldi and Arblaster, 2014), or when attempting to recreate moving boundaries such as sea ice extent and snow cover (Collins et al., 2013). Nonetheless, the benefits of pattern

https://doi.org/10.5194/egusphere-2023-2932
Preprint. Discussion started: 26 February 2024

scaling to enable rapid reconstruction of spatial patterns based on global temperature make it an extremely valuable tool for studying, for example, carbon cycle feedbacks using an intermediate complexity climate model (Mercado et al., 2009; Burke et al., 2017).

Other tools are currently being developed to explore the use of pattern scaling for local climate change impacts. The Modular Earth System Model Emulator with spatially resolved output (MESMER; Beusch et al. (2020)) draws on patterns of temperature from CMIP6 models and its extension (MESMER-M; Nath et al., 2022) to this focuses on spatially resolved monthly temperature or extremes (MESMER-X; Quilcaille et al., 2022). MESMER is an emulator of temperature patterns and uses a stochastic representation of natural variability. Goodwin et al. (2020) have also used pattern scaling with the WASP global emulator to look at local temperature projections. Alternatively, the STITCHES system (Tebaldi et al., 2022) presents an option for ESM emulation for impacts research by 'stitching' together ESM output from known scenarios.

Using pattern-scaled climate variables instead of ESM output to drive impacts models therefore offers an opportunity to quickly derive impacts from scenarios. Global mean temperature is readily and efficiently calculated from emissions scenarios using one of a range of climate emulators (Nicholls et al., 2020), which are computationally cheap to run. The regional climate patterns are then scaled by applying global mean temperatures produced from emulators. Bypassing ESMs is particularly useful for assessing novel scenarios, particularly those that are regularly updated (Richters et al., 2022) to address specific questions around Paris agreement compliance and overshoot (Rogelj et al., 2018; IPCC, 2022), or to answer "what-if" questions relating to the Earth's geophysical response (Dvorak et al., 2022). The efficiency and flexibility of emulators allows them to run ensembles in a probabilistic Monte Carlo framework, spanning the range of assessed climate uncertainty with different parameter choices (Nicholls et al., 2021).

Here we present PRIME (Probabilistic Regional Impacts from Model patterns and Emissions): a tool designed to bridge the gap between scenarios and impacts in a computationally efficient manner. PRIME enables the state-of-the-art science to be used throughout the modelling chain starting from the latest scenarios all the way to the simulation of regional impacts. PRIME includes the latest understanding of climate and carbon cycle feedbacks, the latest spatial patterns of climate change, and a leading land-surface model/impacts model. In PRIME we accommodate a broad range of variables in addition to temperature, with a focus on those which are important for impacts assessments. The elements of PRIME are explained in more detail in Section 2. An evaluation of the performance of the framework is provided in Section 3, additional results that are relevant for impacts applications are presented in Section 4, with discussion and conclusions in Section 5.

2 Methods

PRIME is a rapid-response tool designed to explore spatially resolved climate and impacts of scenarios as soon as they are developed. It draws on comprehensive CMIP multi-model ensemble results, but extends these to fill gaps not yet populated by ESMs or impact models and can extend simulations into the future to simulate multi-century response. PRIME produces probabilistic sampling of a range of uncertainties, including global climate and carbon cycle sensitivity and spatial patterns of climate change. It opens the potential to also span perturbed parameter uncertainty in land and impacts models and provides

https://doi.org/10.5194/egusphere-2023-2932
Preprint. Discussion started: 26 February 2024

the ability to propagate constraints onto impacts projections through either prior constraint on parameters or posterior selection of ensemble members.

Figure 1 shows the components that make up the PRIME framework. The starting point is emissions scenarios such as from integrated assessment models (IAMs), which are used to drive the global climate emulator FaIRv1.6.2 (Smith et al., 2018, see Sect. 2.1). FaIR can probabilistically sample uncertainty in climate and carbon cycle response to emissions. Its global mean temperature projections are then used to reconstruct the regional climate change for a number of climate variables using the patterns derived from ESMs (see Sect. 2.2). These regional patterns, along with CO_2 concentrations from FaIR, are used to drive the JULES land surface model, from which various climate impacts can be derived.

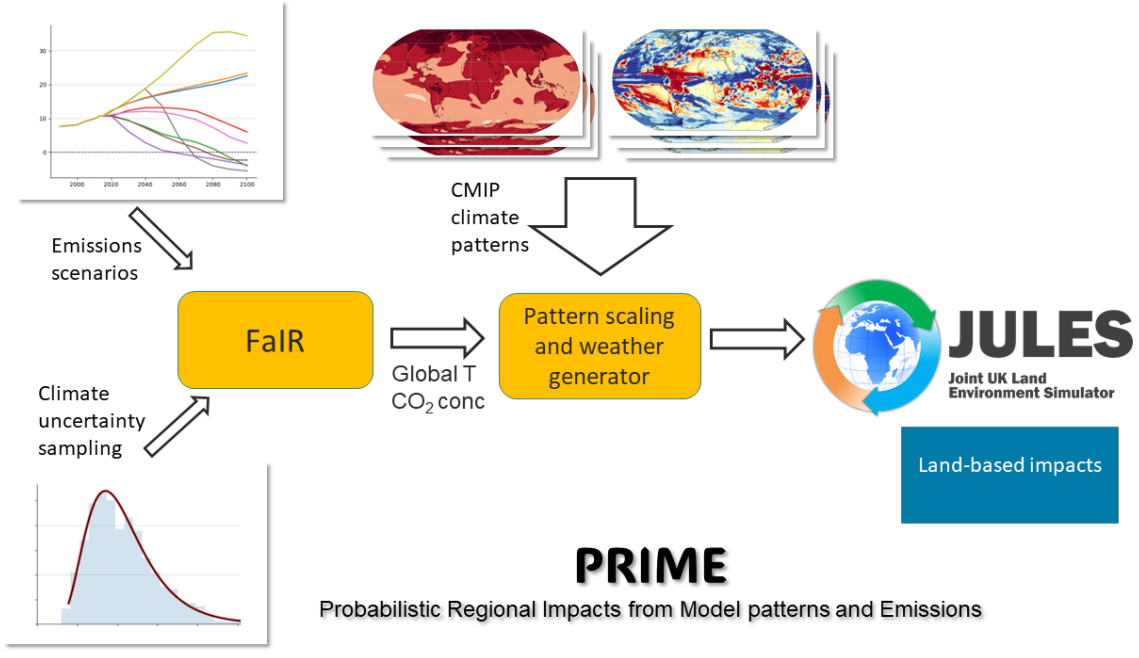

Figure 1. Schematic of the PRIME framework. Emissions scenarios provide input in terms of emissions of CO_2, other greenhouse gases, and aerosols and can be taken from IAMs or idealised experiments. The FaIR climate emulator samples uncertainty from the climate and carbon cycle response to emissions and outputs global temperature and CO_2 concentration. PRIME then scales patterns of climate change from CMIP climate models by the global temperature and uses a weather generator to downscale these to sub-daily driving data for the JULES land surface model. JULES outputs a broad range of land-based impacts-relevant quantities such as gross primary productivity (GPP), Net primary productivity (NPP), vegetation cover, soil moisture and runoff.

2.1 Emulator of Global Temperature change

The Finite-amplitude Impulse Response (FaIR) model is a climate emulator that takes inputs of greenhouse gas and short-lived climate forcer emissions and produces projections of global mean surface temperature (Smith et al., 2018; Leach et al., 2021).

https://doi.org/10.5194/egusphere-2023-2932
Preprint. Discussion started: 26 February 2024

FaIR calculates greenhouse gas concentrations (including CO_2) and effective radiative forcing as intermediate steps. FaIR contains modules that simulate the carbon cycle feedback (changes in uptake of CO_2 by land and ocean sinks with increasing CO_2 emissions and warming), and forcing from aerosols, ozone, land-use change and several other categories of anthropogenic and natural forcings. These relationships in FaIR are designed to capture the large-scale behaviour of complex Earth system models, and are governed by a number of tuneable parameters.

As part of the IPCC AR6 Working Group 1 (The Physical Science Basis of Climate Change: WGI; IPCC, 2021), a large ensemble of FaIR v1.6.2 was produced and constrained to assessed ranges, including uncertainty of several climate indicators, such as present-day warming and Equilibrium Climate Sensitivity (ECS; Forster et al., 2021; Smith et al., 2021). An ensemble of 2237 parameter sets was taken forward and used for assessing emissions pathways derived from IAMs in the Working Group III (Mitigation of Climate Change: WGIII) report (Riahi et al., 2022). We use this ensemble as part of the PRIME framework (Smith, 2022). The climate uncertainty parameters sampled include radiative forcing from different drivers (including aerosols), carbon cycle sensitivities, timescales of climate response to forcing, and climate sensitivity. Typically in PRIME, we reduce the total number of ensemble members by sub-sampling from within the 2237 parameter sets to explore the full range of global temperature sensitivity using several percentiles at 0, 1, 5, 25, 50, 75, 95, 99 and 100%; these are selected using one scenario so that scenarios can be compared against each other.

2.2 Spatial patterns and temporal downscaling of climate change

In PRIME, we use an early version of pattern-scaling developed by Huntingford and Cox (2000). We derive relationships for eight variables (near-surface air temperature, diurnal temperature range, precipitation, shortwave radiation, longwave radiation, near-surface specific humidity, 10m wind speed, and surface pressure) by linear regression at each grid cell, using global mean temperature change as the predictor and anomalies relative to the 1850–1889 mean. Monthly patterns for 34 CMIP6 models (see Supplementary Table S1) were calculated, using the SSP5-8.5 emissions scenario: sampling the CMIP6 ensemble's range of uncertainty. Wells et al. (2023) show that whilst selecting patterns derived from emissions scenarios with radiative forcings closer to the target scenario results in the lowest emulation errors, the best all-round performance is obtained by using a high warming scenario to obtain the patterns, hence our choice of SSP5-8.5. For further detail on the patterns evaluation, see Section 3.2.

The spatial distribution of the meteorological driving data for JULES was reconstructed from the climate patterns multiplied by the global mean temperature change (Section 2.1) superimposed on an observed monthly climatology. The observed monthly climatology was constructed from the daily meteorological data provided by the GSWP3-W5E5 dataset from the ISIMIP3a project (Frieler et al., 2023) for the period 1901–1930. This was regridded to a resolution of N48 with a 3.75° longitude grid size and a 2.5° latitude grid size.

The monthly data was downscaled to hourly data using a weather generator embedded within JULES (Williams and Clark, 2014). At any given location, the daily meteorology was assumed to be the same for every day of the month. The daily data was disaggregated to hourly data by imposing a diurnal cycle on temperature and radiation and allocating the precipitation to a continuous set of timesteps in any particular day. The pressure and wind speed were assumed to be constant throughout the

https://doi.org/10.5194/egusphere-2023-2932
Preprint. Discussion started: 26 February 2024

day and the specific humidity is kept below the specific humidity at saturation.

The diurnal cycle in near surface air temperature was defined using:

$$T = T_o + \frac{\Delta T}{2} cos\Big(\frac{2\pi(t - t_{T_{max}})}{T_{day}}\Big) \quad (1)$$

where T_o and ΔT are the temperature and diurnal temperature ranges respectively. T_{day} is the length of the day, $t_{T_{max}}$ is the time of day when the temperature is highest. $t_{T_{max}}$ is calculated from the following equation which assumes that it occurs 0.15 of a day length after solar noon:

$$t_{T_{max}} = \frac{t_{up} + t_{down}}{2} + 0.15(t_{up} - t_{down}) \quad (2)$$

where t_{up} and t_{down} are sunrise and sunset times.

The downward longwave radiation which includes the diurnal cycle (R_{lw}) is a function of temperature (Huntingford et al., 2010) and is derived assuming black body radiation and that the diurnal cycle of temperature is negligible:

$$R_{lw} = R_{lw,o} + \Big(\frac{4T}{T_o} - 3\Big) \quad (3)$$

where $R_{lw,o}$ is the downward longwave radiation before temporal disaggregation. The downward shortwave radiation which includes the diurnal cycle is the daily mean downward shortwave radiation multiplied by a solar radiation normalisation factor which depends on the position of the sun in the sky at each timestep for each gridbox.

Precipitation was split into 3 types: large-scale rain, convective rain and large-scale snow. The type of precipitation at any particular time depends on the mean daily temperature. If the daily temperature is greater than 293.15 K it is convective rain, between 275.15 K and 293.15 K it is large scale-rain and below 275.15 K it is large scale-snow. This precipitation is divided into events of randomly generated duration. If the maximum precipitation rate in any timestep is greater than 350.0 mm/day, the precipitation is again redistributed to reduce these values to less than the threshold.

2.3 Land Surface and Impacts Model

The Joint UK Land Environment Simulator Earth System (JULES; Best et al., 2011; Clark et al., 2011; Wiltshire et al., 2021) land surface model is a community model used both in standalone model and as the land surface component of the UK Earth System Model (UKESM; Sellar et al., 2019). Here, JULES is used in standalone mode, driven by climate data reconstructed by combining the monthly patterns derived from the ESMs and the global mean temperature change from FaIR. The configuration of JULES used here is denoted JULES-ES (Mathison et al., 2022) and is the configuration used in both UKESM1 (Sellar et al., 2019) and to provide simulations for the Inter-Sectoral Impact Model Intercomparison Project (ISIMIP) in Mathison et al. (2022). In PRIME JULES-ES is also driven by the CO_2 concentration output from FaIR.

https://doi.org/10.5194/egusphere-2023-2932
Preprint. Discussion started: 26 February 2024

JULES-ES has 9 natural plant functional types (PFTs; 5 types of trees, C3 and C4 grasses, and evergreen and deciduous shrubs) and four managed PFTs (C3 and C4 crop and pasture), where the managed PFTs are set to their observed values at 2005. The Top-down Representation of Interactive Foliage and Flora Including Dynamics (TRIFFID) dynamic vegetation model (Cox, 2001) determines the proportion of each PFT present in a grid cell. Nitrogen limitation on ecosystem carbon assimilation is represented in JULES-ES (Wiltshire et al., 2021). External nitrogen inputs are via biological nitrogen fixation and nitrogen deposition, and losses are via leaching and a gas loss term. Nitrogen limitation reduces the carbon-use efficiency of the vegetation via a reduced net primary productivity and can slow soil decomposition. The soil biogeochemistry is represented by a single bulk layer with four soil pools: two litter pools, a microbial biomass pool, and a humus pool each with an equivalent organic nitrogen pool. Inorganic nitrogen is converted from organic nitrogen and can be taken up by the plants.

3 PRIME evaluation

In this section, we evaluate PRIME. In this context, that means that we want to use PRIME to produce land simulations for scenarios where ESMs have not been run, but we can test it in cases where ESM simulations do exist. Here, we use CMIP6 simulated output for a range of different but well known future climate scenarios: SSP1-2.6, SSP5-3.4-OS and SSP5-8.5. We show that PRIME gives close agreement of global temperature and spatial patterns of climate giving us confidence in its ability to be used to project as-yet un-simulated scenarios. We also compare simulated land-surface output from PRIME with that from CMIP6 for ESMs that have reported the required diagnostics.

PRIME has 3 distinct and independent steps, as described in Section 2: (i) timeseries of global temperature are produced from FaIR based on emissions of greenhouse gases and aerosols, (ii) spatial patterns of climate change are constructed from the global temperature based on CMIP simulations, and (iii) these climate patterns are used to drive JULES to simulate land surface outcomes. In this section, we present evaluation of these three steps and at each step assess the agreement with existing output from CMIP6 or the IPCC AR6 assessment.

3.1 Emulation of global temperature change

For the first time, IPCC AR6 was able to apply multiple lines of evidence to constrain future projections of global temperature from the CMIP6 ensemble. As such, the spread of global temperature in 2100 is smaller than if taken from raw CMIP6 ESM output (Lee et al., 2021). We compare the simulated global temperature from PRIME (run with emissions) with the constrained range assessed by IPCC (see Figure 4.11 and Table 4.5 of Lee et al. (2021)) in Figure 2. The FaIR simulations used here do not include solar and volcanic fluctuations, instead focusing on the anthropogenic forcing, which is the main driver of human-induced effective radiative forcing and human-induced warming (Forster et al., 2023). The left panel shows the mean Global mean Surface Air Temperature (GSAT) from FaIR (solid lines) and 5th and 95th percentiles (shaded region). The right panel shows the mean and 5–95th percentile for the period 2090–2100 relative to 1850–1900 for each SSP scenario (we include the same scenarios here to enable comparison with the same plot in the IPCC report): SSP1-1.9, SSP1-2.6, SSP2-4.5, SSP3-7.0

https://doi.org/10.5194/egusphere-2023-2932
Preprint. Discussion started: 26 February 2024

and SSP5-8.5 for FaIR end of century GSAT values and the IPCC constrained values. The end of century ranges in PRIME are close to the IPCC ranges with the timeseries and model spread consistent with the IPCC constrained range.

The uncertainty in projected global mean temperature arises from uncertainty in both physical and biogeochemical feedbacks like the carbon cycle. We know atmospheric CO_2 is an additional direct driver of impacts, therefore this is included in PRIME as a secondary forcer to the meteorology in JULES-ES. PRIME samples the joint distribution of CO_2 and global temperature from the constrained FaIR ensemble. Figure 3 shows that the ensemble members selected span the distribution for SSP5-8.5 (similarly the joint distribution of CO_2 and temperature are also shown in the Supplementary information Fig. S1 for SSP1-2.6; left and SSP5-3.4-OS; right). The FaIR ensemble samples uncertainty in carbon cycle feedback strength with climate sensitivity resulting in a joint distribution of global mean temperature and atmospheric CO_2 concentration. High atmospheric CO_2 concentrations are consistent with a lower climate sensitivity and vice versa. As our primary aim is to sample future impacts associated with uncertain future temperature outcomes, we subsample the 2100 FaIR temperature distribution for the impacts modelling. This results in a co-sampling of CO_2 levels that does not span the full uncertainty in resulting CO_2 concentrations. This is not a limitation of PRIME - other applications could use a different sampling strategy or use the full ensemble of 2237 members.

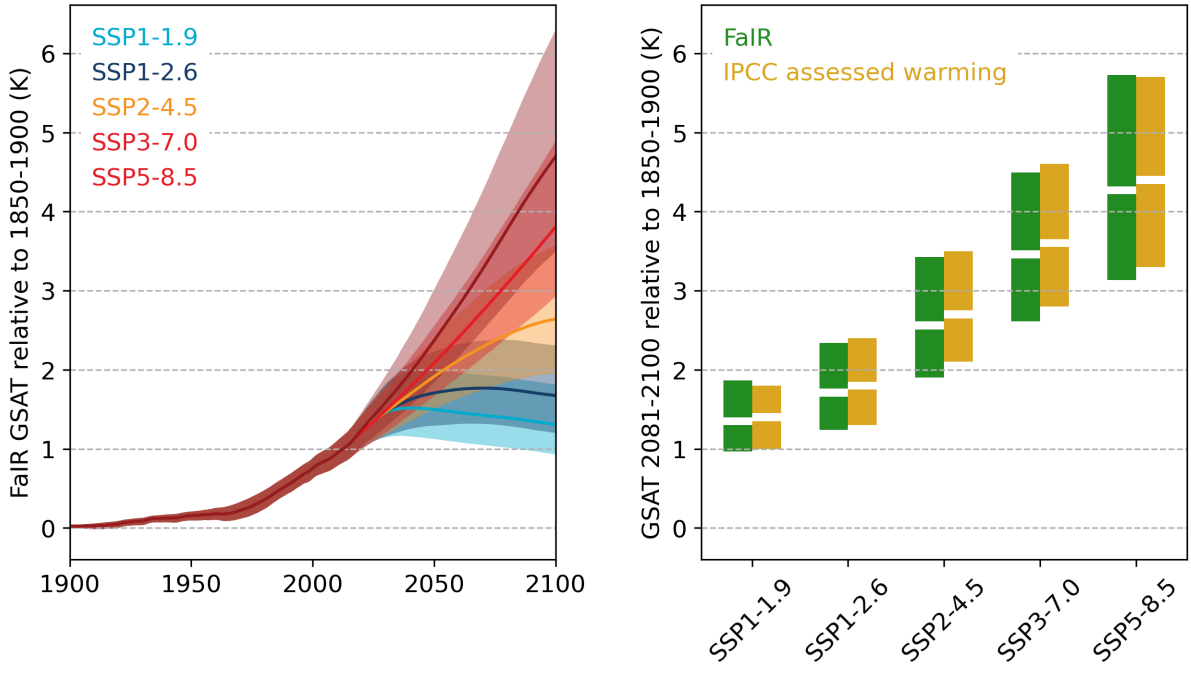

Figure 2. (a) Projected global temperature from FaIR for five SSP emissions scenarios, and (b) comparison of end-of-century (2080–2100) mean warming from FaIR (green) and IPCC AR6 assessment (yellow; Figure 4.11 and Table 4.5 of Lee et al. (2021))

.

https://doi.org/10.5194/egusphere-2023-2932
Preprint. Discussion started: 26 February 2024

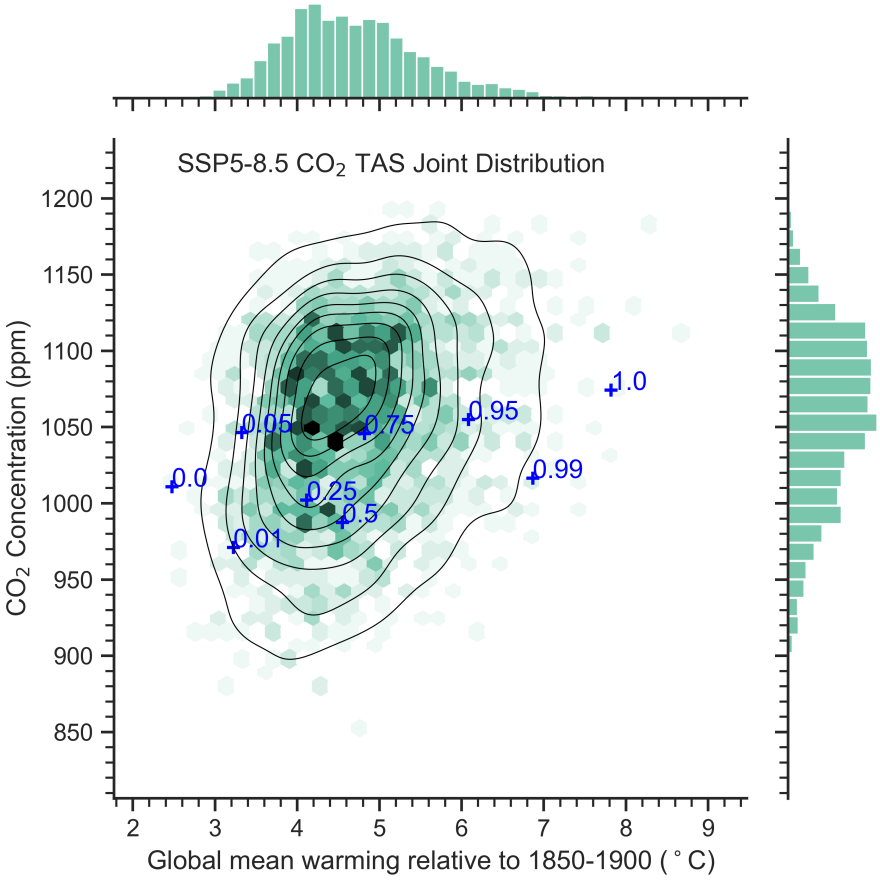

Figure 3. Joint frequency distribution of global temperature rise and CO_2 for SSP5-8.5 emissions and the sub-selected percentiles (blue crosses) used to drive the JULES impacts model. Shades of green denote the density of points with individual histograms are above and to the right of the main panel. 10% confidence intervals are shown by the contours.

3.2 Spatial patterns of climate change

Climate patterns were evaluated against CMIP6 simulations of their corresponding models. Alongside global comparison, four example regions are chosen to test the pattern evaluation at regional scales: the Amazon basin, the Siberian forest, India and the United States of America. These regions span tropical and boreal ecosystems, temperate regions and a region dominated by a Monsoon climate. The climate patterns were evaluated against CMIP6 runs of the SSP5-8.5, SSP1-2.6 and SSP5-3.4-OS scenarios.

Climatologies of each CMIP6 model were calculated by taking the mean of the period 1850–1889 inclusive. Anomalies were then calculated by subtracting the climatologies from the spatiotemporal CMIP6 datasets, ensuring that the variants of the

https://doi.org/10.5194/egusphere-2023-2932
Preprint. Discussion started: 26 February 2024

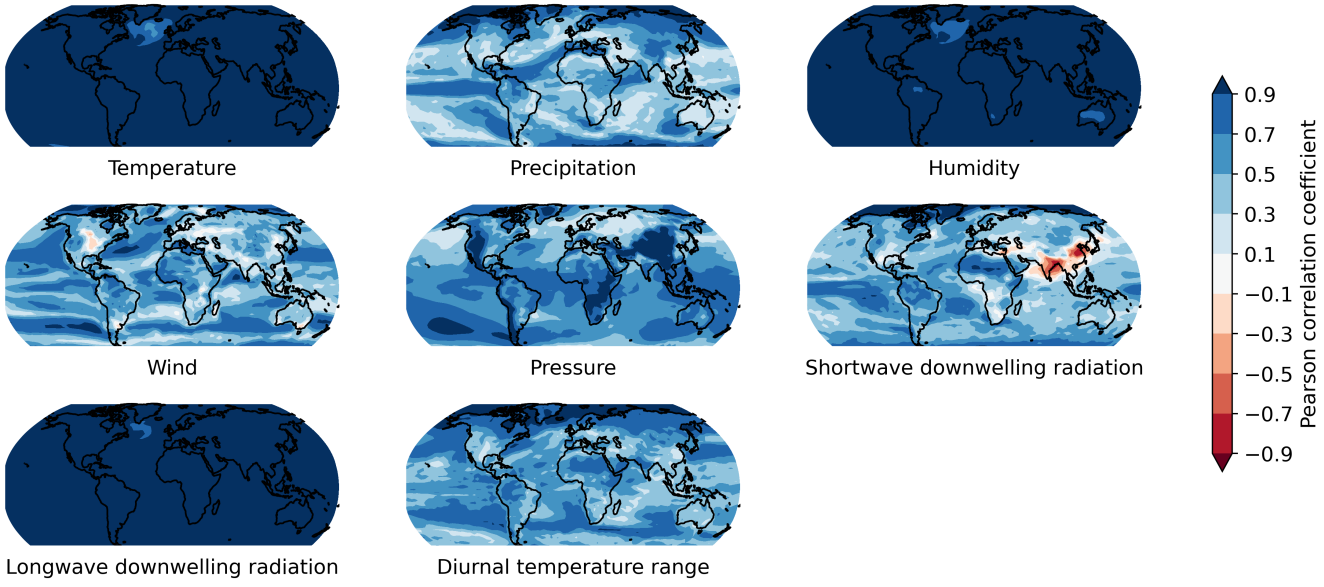

Figure 4. Evaluation of pattern scaling compared to CMIP6 multi-model mean changes for each JULES input variable (labelled). Pearson correlation coefficients are averaged over model and month for each pattern variable.

historical runs matched those of the scenarios. To compare against these, predicted patterns for each ESM were compiled by multiplying annual mean GSAT data by pattern values at each grid point (see Methods, Section 2.2), creating a spatiotemporal dataset of anomalies for each variable (see Table 1). The predicted patterns were then evaluated against the anomaly datasets from CMIP6.

We evaluate both the ability of PRIME pattern scaling to replicate the CMIP6 ESM and multi-model mean values and across-model performance of PRIME to reproduce the range of results across CMIP6 ESMs. For each gridpoint, we calculate the Pearson correlation coefficient of the relationship between the scaled pattern for each variable and the CMIP6 multi-model mean, using decadal means (Figure 4). High correlation coefficients show that across the ensemble there is a relationship with temperature that we use to make spatial projections of the JULES meteorological forcers. Temperature, specific humidity and longwave radiation have the strongest predictability with global temperature, with mean correlation coefficient values over global-land of 0.99, 0.98, 0.99, respectively which show strong spatial consistency and are largely statistically significant (Figure S2). Precipitation, wind, pressure, shortwave radiation and diurnal temperature range all show weaker, but strongly significant positive scores at 0.52, 0.44, 0.69, 0.41 and 0.58 respectively. These variables also show a stronger spatial variation, with for instance, precipitation showing a weak correlation over Australia but stronger over the high latitudes. This can also be seen in the lower number of statistically significant relationships for individual months and models (Figure S2).

To test whether pattern scaling can reproduce simulated changes under different scenarios, we calculate the patterns of each variable change for 2080–2100. These are shown in Figure 5 for SSP5-8.5, with SSP1-2.6 and SSP5-3.4-OS in Figures S3 and S4 of the Supplementary information, respectively. Predicted patterns were calculated by multiplying the 2080–2100 mean

https://doi.org/10.5194/egusphere-2023-2932
Preprint. Discussion started: 26 February 2024

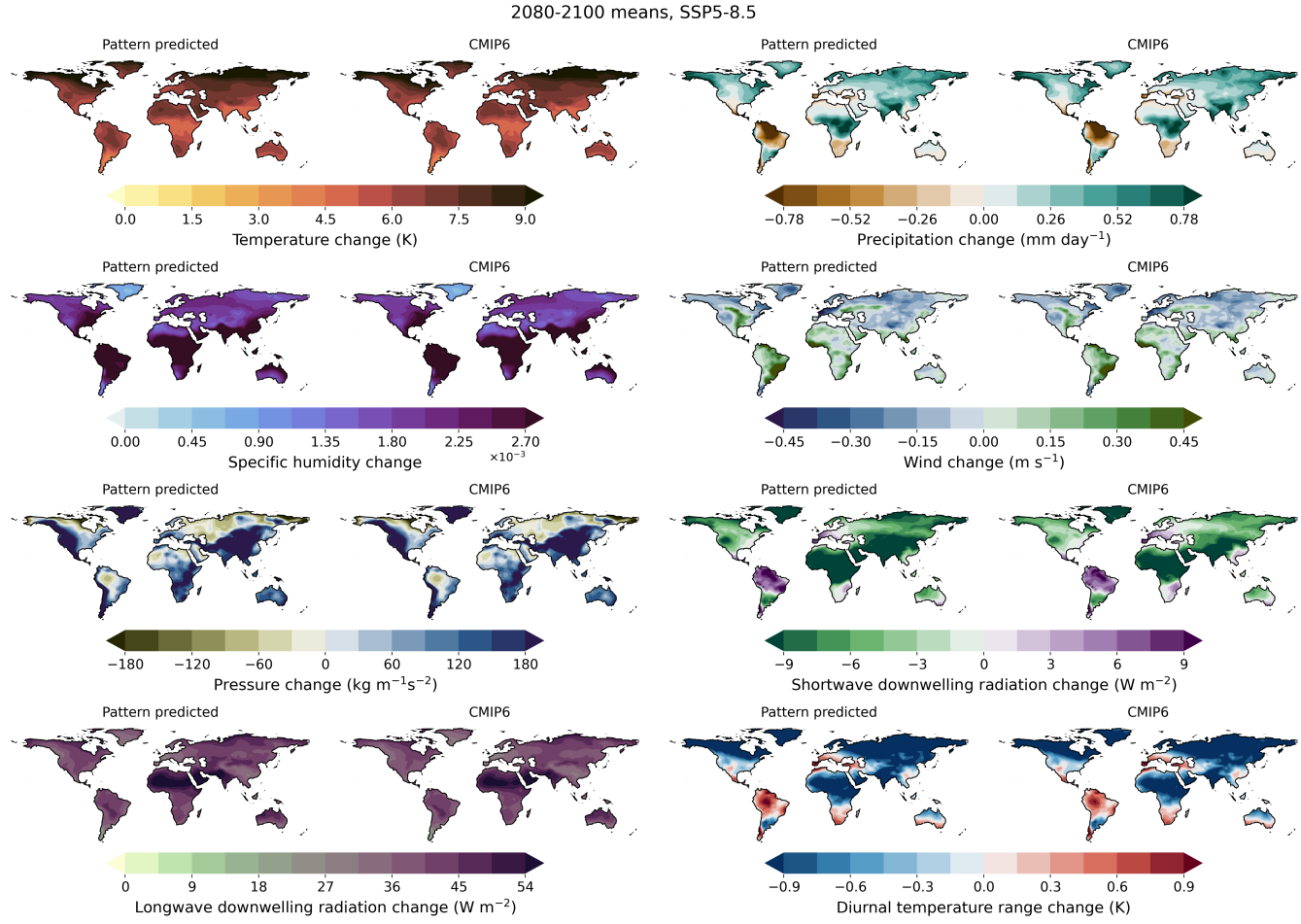

Figure 5. End of century changes (2080–2100) in each JULES input variable (labelled) for SSP5-8.5 predicted by patterns (left hand side of each variable panel) compared to CMIP6 values (right hand side of each variable panel). Plots shows the multi-model means.

GSAT anomaly for each model by the corresponding model pattern, then taking the mean of all model predictions. Overall, the major areas of change predicted by the patterns correspond well to CMIP6 predicted changes. The Pearson correlation and the RMSE are given in Table 1 for each JULES input variable. RMSE is a standard measure of the error in the predicted variable relative to the mean change. Overall, the pattern scaling captures the pattern of change well for most variables, with SSP5-8.5 having the greatest agreement as expected because this is the scenario with the strongest climate change signal, and was used to generate the patterns. Some patterns, such as wind, have substantially greater error, but JULES is known to be less sensitive to these. The relative error increases in the lower scenarios related to the need to predict a smaller signal. However, the high correlations and low RMSEs give us confidence to apply the pattern scaling to different scenarios including stabilisation and overshoot pathways.

https://doi.org/10.5194/egusphere-2023-2932
Preprint. Discussion started: 26 February 2024

Table 1. Summary table for evaluation section: Pearson correlation coefficient (labelled Pearson) and Root Mean Square Error (labelled RMSE) between multi-model mean pattern predicted and CMIP6 end of century values on land across the globe for each variable. Pearson r-values and RMSE are spatially aggregated across months and models.

Variable	Units	CMIP abbreviation	SSP1-2.6		SSP5-3.4-OS		SSP5-8.5	
JULES inputs			Pearson	RMSE	Pearson	RMSE	Pearson	RMSE
Temperature	$^{\circ}C$	tas	0.95	0.42	0.97	0.4	0.99	0.31
Specific Humidity	g kg^{-1}	huss	0.95	0.0002	0.97	0.0001	0.99	0.0001
Precipitation	mm day^{-1}	p	0.83	0.16	0.89	0.16	0.97	0.14
Wind	m s^{-1}	sfcWind	0.89	0.11	0.93	0.11	0.98	0.076
Pressure	kg m^{-1} s^{-2}	ps	0.93	30.8	0.96	29.9	0.99	23.4
Shortwave radiation	W m^{-2}	rsds	0.86	2.7	0.88	2.83	0.97	2.94
Longwave radiation	W m^{-2}	rlds	0.92	2.4	0.95	2.5	0.99	1.81
Diurnal temperature range	$^{\circ}C$	tasmax-tasmin	0.91	0.25	0.93	0.25	0.99	0.20

To evaluate if PRIME pattern scaling can also reproduce the range of different changes across the CMIP6 ensemble, we compare timeseries and end of century predicted changes across CMIP6 ESMs for four regions. The multi-model mean pattern, per °C of warming, is shown in the central map for temperature (Fig. 6) and precipitation (Fig. 7). Burton et al. (2020) show that temperature and precipitation are the most important drivers of land-surface processes. The other six variables needed to drive JULES are presented in the Supplementary information (Figures S5 to S10). For each region, the figures show timeseries of change for that region as a shaded plume of CMIP6 output (blue) and predicted by pattern-scaling (pink). The end-of-century values for each CMIP6 model individually are shown as a scatter-plot for each scenario to illustrate the agreement between pattern-scaled and actual values. For temperature (Fig. 6) the range of future projections across CMIP6 models spans approximately 5-10 °C warming by 2100 under SSP5-8.5 for each region, with high-latitudes warming more than the tropics as expected. The PRIME pattern-scaled ensemble does a good job of reproducing this range of projections across the CMIP6 ensemble, with points lying close to the 1-to-1 line for all regions and scenarios. Correlation coefficients for between-model predictions exceed 0.93 for all regions and scenarios (Table 2), with SSP5-8.5 fitted the best. This is expected as the patterns were derived from this scenario. This gives confidence that the pattern scaling accurately reproduces the spread of results, model-by-model of the CMIP6 ensemble.

Results for precipitation (Fig. 7) also show good agreement, but some mismatches appear, as precipitation is more variable in space and time than temperature as seen in the higher error characteristics in the pattern scaling. Nevertheless, PRIME well predicts the signal of increasing precipitation over the United States, Siberia and India and reduced rainfall over the Amazon Basin. Again, the range and spread of results across the CMIP6 ensemble are well matched, and correlation coefficients are shown in Table 3.

https://doi.org/10.5194/egusphere-2023-2932
Preprint. Discussion started: 26 February 2024

Table 2. Pearson correlation coefficient (Pearson) and Root Mean Square Error (RMSE in °C) between pattern predicted and CMIP6 end of century temperature change. Average values over region of interest compared to its CMIP6 equivalent by model. All statistically significant (p-values <0.05).

Region	SSP1-2.6		SSP5-3.4-OS		SSP5-8.5	
	Pearson	RMSE	Pearson	RMSE	Pearson	RMSE
Amazon	0.96	0.27	0.98	0.22	1.0	0.13
Siberia	0.93	0.33	0.98	0.28	0.99	0.23
USA	0.95	0.21	0.98	0.21	0.99	0.21
India	0.93	0.29	0.97	0.21	0.98	0.37

Table 3. Pearson correlation coefficient (Pearson) and Root Mean Square Error (RMSE in mm day^{-1}) between pattern predicted and CMIP6 end of century precipitation change. Average values over region of interest compared to its CMIP6 equivalent by model. All statistically significant (p-values <0.05).

Region	SSP1-2.6		SSP5-3.4-OS		SSP5-8.5	
	Pearson	RMSE	Pearson	RMSE	Pearson	RMSE
Amazon	0.77	0.12	0.85	0.11	0.98	0.079
Siberia	0.86	0.045	0.96	0.036	0.99	0.022
USA	0.75	0.065	0.83	0.056	0.96	0.037
India	0.87	0.094	0.93	0.081	0.94	0.13

Across-model spread of the other variables (Figures S5 to S10 of the Supplementary information) is also well captured by PRIME pattern scaling. Changes in humidity (Fig. S5) are well reproduced, while wind speed changes (Fig. S6) has mixed skill being poorly captured over United States, despite changes in surface pressure (Fig. S7) being well reproduced for all regions. The most notable departure of predicted and actual changes occurs for surface downwelling shortwave radiation (i.e. incoming solar radiation shown in Fig. S8). For all regions and scenarios, the end-of-century values match well, but the significant dip in shortwave radiation during the historical period is not seen at all in the predicted patterns. This period of "global dimming" (Wang Z; Stanhill and Cohen, 2001) is well known to be caused by anthropogenic aerosols and cannot be replicated by scaling global temperature. Features such as this are an obvious limitation of a pattern scaling approach which does not account for different regional patterns from different climate forcers such as aerosols. Finally, changes in upwelling long-wave radiation (Fig. S9) and diurnal temperature range (Fig. S10) are well captured across regions and scenarios by the PRIME pattern scaling.

In conclusion, the patterns both for each CMIP6 ESM and the range of changes across ESMs are generally well reproduced by the PRIME pattern scaling technique. This is true for each of the four distinct regions and three very different emissions scenarios.

https://doi.org/10.5194/egusphere-2023-2932
Preprint. Discussion started: 26 February 2024

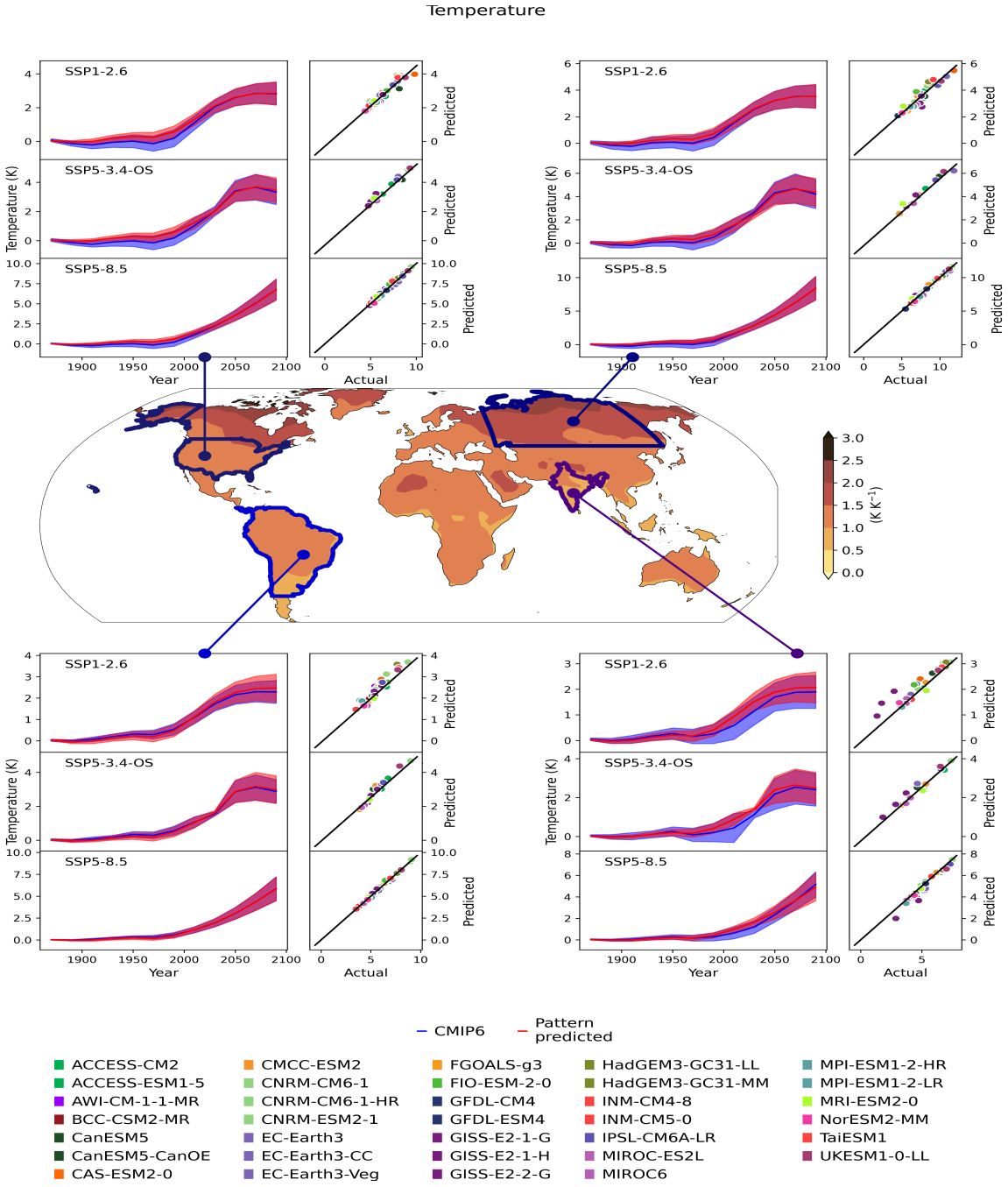

Figure 6. The central map shows the temperature pattern (where there is no hatching indicates that the models tend to agree on the sign of the change and with hatching to show where the models tend to disagree on the sign of the change), and subpanels for each region: North America, Siberia, South America and South Asia. The region subpanels show the temperature timeseries (left subpanel) and scatter plots (right subpanel) for each scenario; top: SSP1-2.6, middle: SSP5-3.4-OS and bottom: SSP5-8.5. The timeseries shows the PRIME patterns (blue plume) and the CMIP6 patterns (red plume). The scatter plots show the end of century values predicted by PRIME vs CMIP6 actual values for each model with the model colours shown at the bottom of the figure.

https://doi.org/10.5194/egusphere-2023-2932
Preprint. Discussion started: 26 February 2024

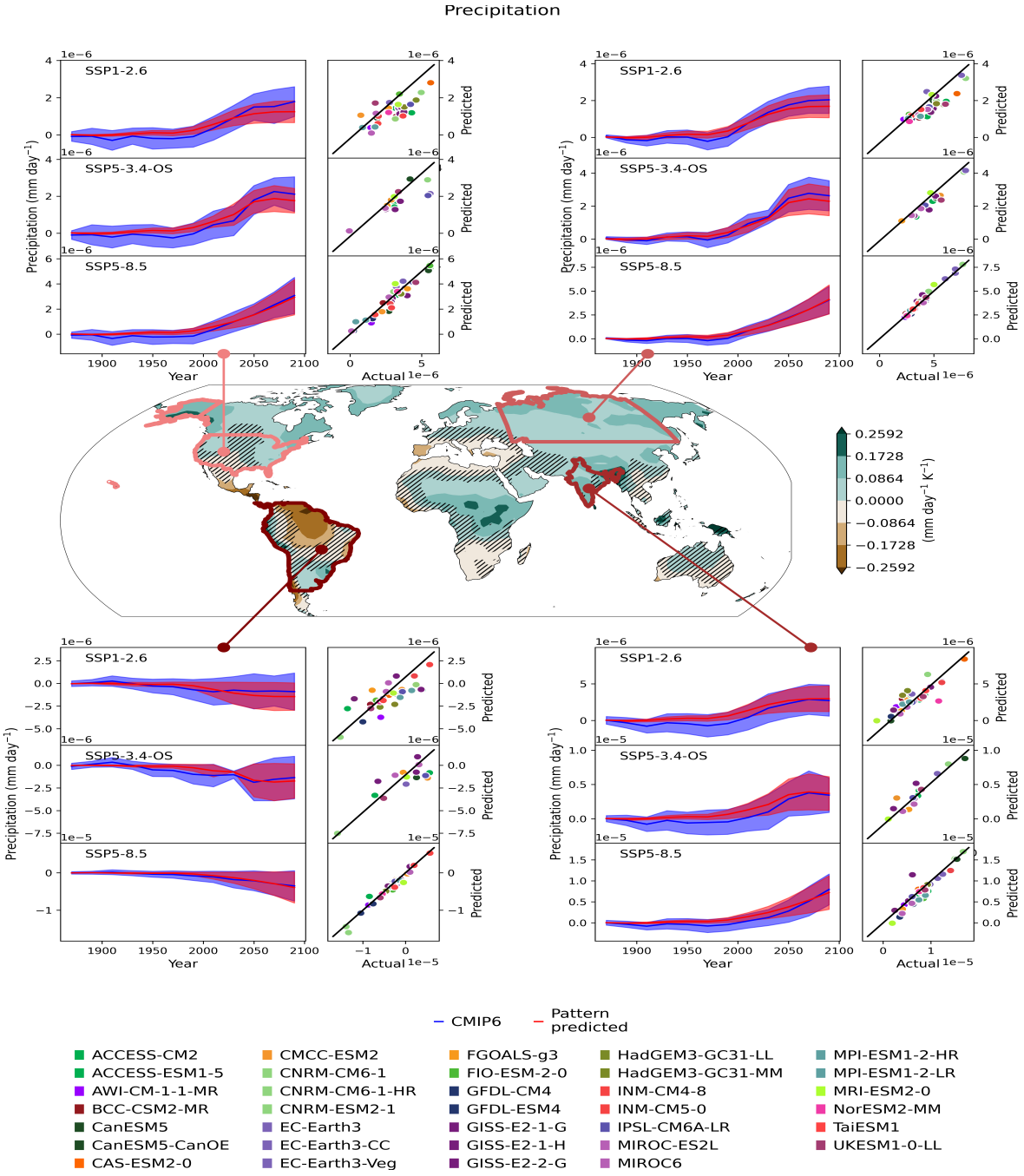

Figure 7. The central map shows the precipitation pattern (where there is no hatching indicates that the models tend to agree on the sign of the change and with hatching to show where the models tend to disagree on the sign of the change) and subpanels for each region: North America, Siberia, South America and South Asia. The region subpanels show the precipitation timeseries (left subpanel) and scatter plots (right subpanel) for each scenario; top: SSP1-2.6, middle: SSP5-3.4-OS and bottom: SSP5-8.5. The timeseries shows the PRIME patterns (blue plume) and the CMIP6 patterns (red plume). The scatter plots show the end of century values predicted by PRIME vs CMIP6 actual values for each model with the model colours shown at the bottom of the figure.

https://doi.org/10.5194/egusphere-2023-2932
Preprint. Discussion started: 26 February 2024

3.3 Land Surface and Impacts Simulation

The final section of the PRIME evaluation shows the results using the FaIR produced projections of global mean surface temperature together with the scaled climate patterns, to drive the JULES land surface model. The JULES step of PRIME is evaluated using two climate variables as examples of output produced by most ESMs. End of century changes projected by PRIME are compared against the equivalent ensemble mean CMIP6 data. The example variables considered help us assess the carbon and hydrological cycles: Gross Primary Productivity (GPP), which is the gross rate of accumulation of carbon via photosynthesis, and runoff (mrro), which is the excess water not absorbed by soils and accumulated by water sources.

For this stage of evaluation, we do not expect as good a match with CMIP6 outputs as obtained for the driving climate variables in Section 3.2. This is because PRIME uses the JULES land-surface model which will differ from the embedded land schemes in the different CMIP6 ESMs. We perform this comparison for two example variables to demonstrate the extent to which the PRIME framework can reproduce the range of simulated land behaviour from CMIP6, but cannot expect a perfect match. Future work to include other land models or perturbed parameter ensembles of JULES would help address potential mismatches.

Figure 8 shows the multi-model mean projected end of century changes in GPP and runoff in the SSP5-8.5 scenario using both the PRIME framework and CMIP6. Figures S11 and S12 in the Supplementary information show the equivalent results for scenarios SSP1-2.6 and SSP5-3.4-OS. The similarity in the predicted spatial patterns can be seen, where in the majority of regions, PRIME matches the pattern of change projected by CMIP6. As we did for climate patterns, we evaluate within and across CMIP6 ESMs. Table 4 presents the Pearson correlation coefficients between PRIME and CMIP6 for each output variable, where consistent values of 0.52 (GPP) and 0.51 (runoff) are found for SSP5-8.5. Some deviations are seen between the projections; for example, PRIME projects greater magnitudes of change in both runoff and GPP in the tropical regions compared to CMIP6 (Fig. 8). To put these changes into context from a carbon perspective, PRIME exhibits an end of century global increase in GPP in SSP5-8.5 of 77 GtC yr^{-1}, while CMIP6 increases by 70 GtC yr^{-1}, compared to pre-industrial.

Table 4. Summary table for JULES outputs: Pearson correlation coefficient between pattern predicted and CMIP6 end of century values on land across the globe.

Variable	CMIP abbreviation	SSP1-2.6	SSP5-3.4-OS	SSP5-8.5
JULES outputs				
Gross primary productivity	gpp	0.44	0.39	0.52
Runoff	mrro	0.42	0.48	0.51

Across CMIP6 models, projections are compared in the four specific regions (Amazon, Siberia, USA and India) for both variables (Supplementary Figures S13-S16). PRIME-simulated GPP and runoff can be compared on a model-by-model basis. The results shown in figures in the Supplementary information (Figures S13-S16) for each region show CMIP6 output for each ESM and the corresponding PRIME simulated output from JULES using the climate patterns from the same ESM. For GPP (top row in Supplementary information Figures S13-S16), the PRIME-simulated changes are typically simulated well,

https://doi.org/10.5194/egusphere-2023-2932
Preprint. Discussion started: 26 February 2024

300 although JULES has a tendency to simulate greater increases in GPP than many of the CMIP6 models. A couple of CMIP6 ESMs clearly stand-out. The blue/green coloured lines showing the CNRM and MPI variants in CMIP6 consistently simulate greater increases in GPP than JULES. This does not signal an error in PRIME, just that the different land models simulate different sensitivity to future climate changes. PRIME does, though, mainly reproduce the signal and spread of GPP for all regions and scenarios simulated by CMIP6.

305 Runoff for three of the four regions is well reproduced in PRIME (bottom row in Supplementary information Figures S13-S16), where: Siberia (Figure S14), United States (Figure S15) and India (Figure S16) all see steady increases in runoff consistent with increases in precipitation in those regions. JULES output agrees with these changes of simulated magnitude and spread. The Amazon basin region (Figure S13) though exhibits some notable differences. Figure 7 (bottom left) shows a range of precipitation responses over the Amazon with an overall consensus of a drying signal (see also Lee et al. (2021)). The 310 JULES outputs though, whilst spanning a similar range of reduced runoff, also show an increase in runoff when forced with some ESM patterns to an extent not shown by the CMIP6 models themselves. The reason for this is not known, but we note that in this case, future projections of Amazon runoff in PRIME show a wider spread than CMIP6 ensemble. These comparisons allow us to confidently use the PRIME framework to assess impacts from scenarios for which ESM simulations do not exist.

4 PRIME Impacts outputs

315 In this section, we present examples of how the PRIME framework can be used to assess climate impacts. Even though the SSP scenarios have been simulated by many ESMs in CMIP6, only a subset simulate the terrestrial carbon cycle (Arora et al., 2020), and very few simulate interactive dynamic vegetation (Pugh et al., 2018). Hence it is novel to show a full probabilistic range of the possible spread of simulated carbon balance (represented by Net ecosystem productivity, NEP) and changes in tree fraction.

320 In response to SSP5-8.5 (Figure 9), terrestrial carbon storage increases almost everywhere in the multi-model mean with positive NEP (top row) especially evident in forested areas. The higher CO_2 concentration in the atmosphere drives enhanced vegetation photosynthesis (GPP; Fig. 8), which increases more than any loss from accelerated decomposition. This outweighs any detriment to vegetation productivity from changes in climate except in a few small regions such as southern Brazil. There is, though, significant spread across members with most regions showing potentially positive and negative NEP changes by 325 2100. This highlights the need for a probabilistic sampling of uncertainty not possible from a limited number of carbon-cycle ESMs. We note that this configuration of JULES does not include representation of fire which has been shown to improve GPP and vegetation distribution in ISIMIP2b simulations (Mathison et al., 2022). In addition, this configuration does not include permafrost carbon dynamics which could substantially alter this result as thawing of frozen ground in the high latitudes is expected to mobilise large amounts of organic carbon (Chadburn et al., 2017; Burke et al., 2018; Varney et al., 2023). Both fire 330 and permafrost carbon dynamics are part of planned future JULES configurations to be implemented in UKESM and therefore will be part of future versions of PRIME.

https://doi.org/10.5194/egusphere-2023-2932
Preprint. Discussion started: 26 February 2024

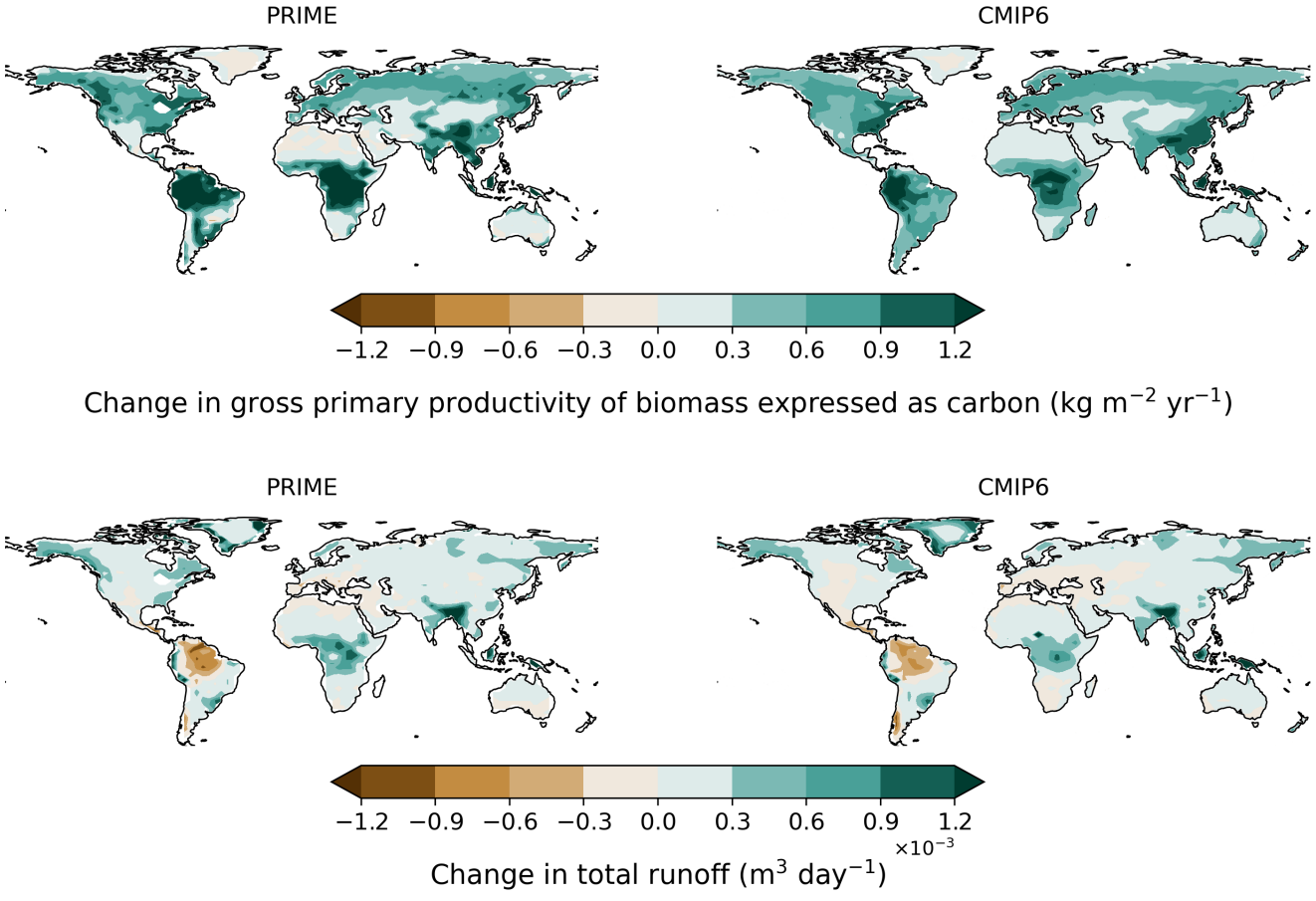

Figure 8. Maps comparing the multi-model mean projected end of century changes (2080–2100) for SSP5-8.5 in GPP (top) and runoff (bottom) from PRIME (left hand side) compared to CMIP6 (right hand side)

Accordingly, tree fraction increases in all regions (Fig. 9, bottom row). This is robust for India, Siberia and United States with relatively small spread compared to the mean signal of increased tree cover. In the Amazon region some ensemble members see a stabilisation and even beginning of loss of tree cover by 2100 as the effects of severe climate change counter the benefits due to elevated CO_2.

Jones et al. (2023) assessed CMIP6 carbon cycle projections against present day observations and also saw increases in biomass and total terrestrial carbon storage in all regions throughout the 21st century for SSP3-7.0. That study could not assess changes in vegetation cover as so few CMIP6 models represent dynamic vegetation. PRIME allows us to go beyond CMIP6 results to analyse impacts on vegetation dynamics and ecosystem composition as well as carbon balance.

https://doi.org/10.5194/egusphere-2023-2932
Preprint. Discussion started: 26 February 2024

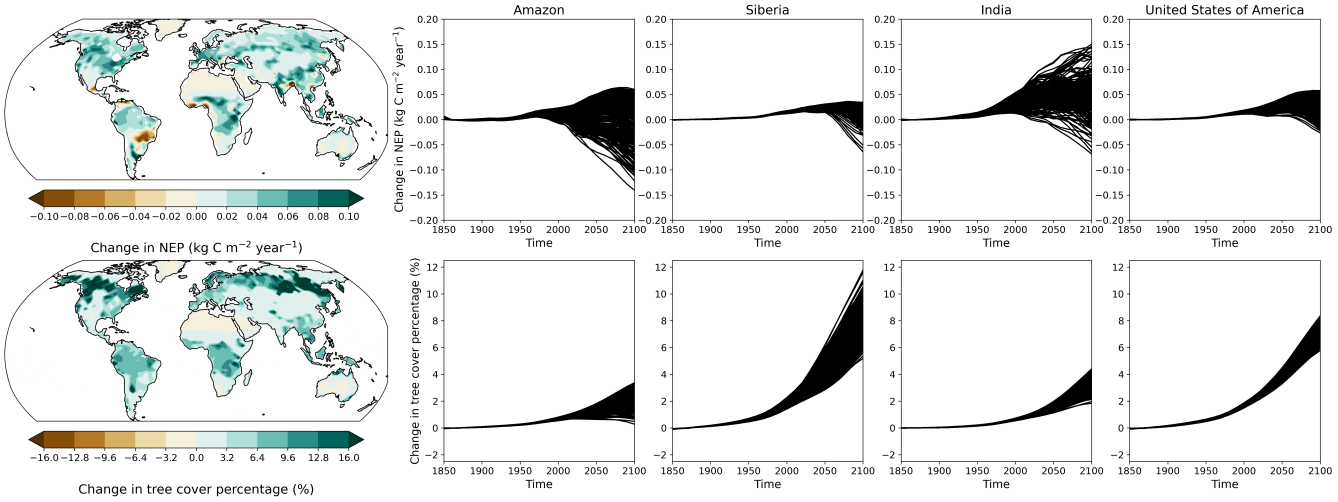

Figure 9. Maps of net ecosystem production (top) and tree fraction (bottom) with timeseries showing the median and uncertainty ranges for each study region: Amazon, Siberia, India and the USA (labelled) between 1850–2100.

5 Discussion and Conclusions

In this study, we document and evaluate the PRIME framework for the first time thereby providing capability for rapid probabilistic regional impacts assessments for any global emissions scenario to be produced in a fraction of the time it takes to run an ESM, being able to run hundreds of simulations in just a few days. We have shown that PRIME reproduces CMIP6 results for a range of SSP scenarios that have been simulated by full complexity ESMs, and in doing so demonstrated that the PRIME framework is fit for purpose.

The PRIME framework allows different sources of uncertainty to be quantified. FaIR provides a constrained probabilistic ensemble capturing the uncertainty in climate response, this is informed by the best available science from the IPCC, and can be easily refined or varied to sample any given range of global sensitivity. The advantages of an emulator like FaIR are its efficient run time and ability to provide projections for any emissions scenario outside of those run by ESMs. FaIR is very flexible and can be readily configured to run multiple scenarios, use multiple parameter sets or simulate idealised profiles as well as realistic scenarios and pathways.

The uncertainty from the full CMIP6 range of simulated patterns is provided through the construction of spatial patterns of change. It is widely accepted that the spatial patterns of change of many climate variables approximately scale with global temperature and are less dependent on a particular scenario or pathway (Mitchell, 2003; James et al., 2017; Tebaldi and Knutti, 2018; Arnell et al., 2019). As such, it is therefore possible to construct future projections of the spatial pattern of climate change given a pathway of global temperature change. This technique of "pattern scaling", when calibrated against a wide range of climate model, enables a rapid assessment of the range of climates for a given trajectory of global temperature.

https://doi.org/10.5194/egusphere-2023-2932
Preprint. Discussion started: 26 February 2024

Studies such as King et al. (2020) have shown changing spatial patterns of climate on long timescales as the system begins to equilibrate following an initial transient period, but experience with the MESMER tool has shown only marginal improvement when additional predictors of patterns are added to global temperature, with the simple, conventional pattern scaling approach showing significant skill with errors typically much smaller than inter-model spread (Beusch et al., 2022).

Pattern-scaling is a powerful methodology which has grown from its original intended purpose of providing a technique to allow extension of the relatively few computationally intensive simulations by ESMs to a broader remit. However there are two main limitations of this methodology. First, by definition, pattern scaling assumes the local and monthly changes in climate to be linear in global warming. Yet many studies suggest that the climate system may contain "tipping points" where strong non-linearity implies there may be future times when there are strong responses of Earth system components to relatively small additional increases in greenhouse gases (e.g., McKay et al., 2022). Linear scaling will not capture such rapid changes if they impact near-surface meteorology, although investigation of ESMs reveals relatively few instances of rapid change (Drijfhout et al., 2015). Although the use of pattern-scaling can currently only offer a linear interpretation of local and seasonal near-surface meteorological response to increasing greenhouse gases, the inclusion in PRIME of the full JULES land surface model does offer the opportunity to investigate in detail the risk of tipping points in land ecosystem response because JULES includes aspects of plant physiology and vegetation dynamics that are strongly nonlinear. A second limitation of pattern-scaling is that it does not resolve local land-atmosphere feedbacks and so will not capture in full the effects of major alterations to the land surface on near-surface meteorology. Such feedbacks may occur by the addition of new processes to land simulations that adjust substantially land-atmospheric exchanges of sensible or latent heat flux. Development of techniques to include such local feedbacks will form the basis of future research.

One of the main advantages of the PRIME framework is its flexibility, with the simple coupling between components lending itself to future couplings using other downstream models. For example, adding other models such as one for sea level rise or air quality to this framework would expand the scenario and climate output to get a rapid response of a broader range of impacts beyond land. Currently, we include just one land model, but other land models could be included in addition to JULES to capture the structural uncertainty in land models as well. It is also worth noting that the methods for downscaling to subdaily timescales in the form of the weather generator in JULES could benefit from more modern approaches which have not yet been investigated herein.

Overall we have shown PRIME faithfully reproduces the climate response to a range of emissions scenarios spanning global temperature in close agreement with IPCC assessments, capturing a range of 34 state-of-the-art Earth system models and simulates a range of land-surface outcomes and impacts. This gives us confidence that PRIME is an ideal tool to use for rapid and probabilistic assessment of novel scenarios, allowing unprecedented ability to quantify societally-relevant climate impacts.

6 Supplementary Information

Supplementary information provided in separate pdf file called 'Supplementary_for_PRIME_doc_paper_submitted_071223.pdf'

https://doi.org/10.5194/egusphere-2023-2932
Preprint. Discussion started: 26 February 2024

Code availability. FaIR v1.6.2 is available from the Python Package Index at https://pypi.org/project/fair/1.6.2/, on GitHub at https://github.com/OMS-NetZero/FAIR/tree/v1.6.2, and at https://doi.org/10.5281/zenodo.4465032. Calibration data for FaIR v1.6.2 is available from https://doi.org/10.5281/zenodo.6601980. Climate patterns calculation code is available from https://zenodo.org/records/10635588.

Ticket has been opened to share the JULES code with reviewers of this manuscript.

 The software is provided by the Met Office to the topical editor at Geoscientific Model Development under the software licence for peer review (use, duplication or disclosure of this code is subject to the restrictions as set forth in the aforementioned software licence for peer review). The software is provided to facilitate the peer review of this paper, "A rapid application emissions-to-impacts tool for scenario assessment: Probabilistic Regional Impacts from Model patterns and Emissions (PRIME)", and should be used and distributed to authorised persons for this purpose only. The software is extracted from the Unified Model (UM) and JULES trunks, with the revisions of the MOSRS repositories corresponding to the stated version, having passed both science and code reviews according to the UM and JULES working practices.

Data availability. FaIR output used in PRIME is available from zenodo at this link: https://doi.org/10.5281/zenodo.10524337.
The ESMValTool patterns recipe linked above automatically downloads the CMIP6 data from ESGF https://esgf-node.llnl.gov/projects/esgf-llnl/, and calculates the patterns.
JULES output for the variables shown for each scenario are available from zenodo at this link: https://doi.org/10.5281/zenodo.10634291.

Author contributions. CM, EJB, CH came up with the concept implemented here and contributed to running some of the individual components of the framework. GM created the patterns, EK completed the analysis of the individual components of the framework which make up many of the plots. CS provided expert knowledge on FaIR and CJ and AJW contributed scientific expertise particularly around the carbon cycle and JULES. LKG and LJV contributed to discussions and writing the manuscript. All were involved in bringing the ideas together and writing and commenting on the manuscript.

Competing interests. The authors can confirm they have no competing interests.

Acknowledgements. This work was supported by the Joint UK BEIS/Defra Met Office Hadley Centre Climate Programme (GA01101), the Newton Fund through the Met Office Climate Science for Service Partnership Brazil (CSSP Brazil), the Natural Environment Research Council (NE/T009381/1), and the European Union's Horizon 2020 research and innovation programme under Grant Agreement No 101003536 (ESM2025 - Earth System Models for the Future). N.J.S. acknowledges funding from the Research Council of Norway (project IMPOSE, grant 294930), as well as funding from the Norwegian Research Centre AS (NORCE). C.H. received support under national capability funding as part of the Natural Environment Research Council UK-SCAPE programme (award no. NE/R016429/1). R.M.V. was supported by the European Research Council's Climate–Carbon Interactions in the Current Century project (4C; grant no. 821003). C.S. was supported

https://doi.org/10.5194/egusphere-2023-2932
Preprint. Discussion started: 26 February 2024

by a NERC-IIASA collaborative research fellowship (NE/T009381/1) and the European Union's Horizon Europe research and innovation programme under Grant Agreement No 101081661 (WorldTrans).

https://doi.org/10.5194/egusphere-2023-2932
Preprint. Discussion started: 26 February 2024

References

Arnell, N. W., Lowe, J. A., Bernie, D., Nicholls, R. J., Brown, S., Challinor, A. J., and Osborn, T. J.: The global and regional impacts of climate change under representative concentration pathway forcings and shared socioeconomic pathway socioeconomic scenarios, Environmental Research Letters, 14, 084 046, https://doi.org/10.1088/1748-9326/ab35a6, 2019.

Arora, V. K., Katavouta, A., Williams, R. G., Jones, C. D., Brovkin, V., Friedlingstein, P., Schwinger, J., Bopp, L., Boucher, O., Cadule, P., Chamberlain, M. A., Christian, J. R., Delire, C., Fisher, R. A., Hajima, T., Ilyina, T., Joetzjer, E., Kawamiya, M., Koven, C. D., Krasting, J. P., Law, R. M., Lawrence, D. M., Lenton, A., Lindsay, K., Pongratz, J., Raddatz, T., Séférian, R., Tachiiri, K., Tjiputra, J. F., Wiltshire, A., Wu, T., and Ziehn, T.: Carbon–concentration and carbon–climate feedbacks in CMIP6 models and their comparison to CMIP5 models, Biogeosciences, 17, 4173–4222, https://doi.org/10.5194/bg-17-4173-2020, 2020.

Best, M. J., Pryor, M., Clark, D. B., Rooney, G. G., Essery, R. L. H., Menard, C. B., Edwards, J. M., Hendry, M. A., Porson, A., Gedney, N., Mercado, L. M., Sitch, S., Blyth, E., Boucher, O., Cox, P. M., Grimmond, C. S. B., and Harding, R. J.: The Joint UK Land Environment Simulator (JULES), model description - Part 1: Energy and water fluxes, GEOSCIENTIFIC MODEL DEVELOPMENT, 4, 677–699, https://doi.org/10.5194/gmd-4-677-2011, 2011.

Beusch, L., Gudmundsson, L., and Seneviratne, S. I.: Emulating Earth system model temperatures with MESMER: from global mean temperature trajectories to grid-point-level realizations on land, Earth System Dynamics, 11, 139–159, https://doi.org/10.5194/esd-11-139-2020, 2020.

Beusch, L., Nicholls, Z., Gudmundsson, L., Hauser, M., Meinshausen, M., and Seneviratne, S. I.: From emission scenarios to spatially resolved projections with a chain of computationally efficient emulators: coupling of MAGICC (v7.5.1) and MESMER (v0.8.3), Geoscientific Model Development, 15, 2085–2103, https://doi.org/10.5194/gmd-15-2085-2022, 2022.

Burke, E. J., Ekici, A., Huang, Y., Chadburn, S. E., Huntingford, C., Ciais, P., Friedlingstein, P., Peng, S., and Krinner, G.: Quantifying uncertainties of permafrost carbon–climate feedbacks, Biogeosciences, 14, 3051–3066, 2017.

Burke, E. J., Chadburn, S. E., Huntingford, C., and Jones, C. D.: CO2 loss by permafrost thawing implies additional emissions reductions to limit warming to 1.5 or 2 °C, Environmental Research Letters, 13, 024 024, https://doi.org/10.1088/1748-9326/aaa138, 2018.

Burton, C., Betts, R. A., Jones, C. D., Feldpausch, T. R., Cardoso, M., and Anderson, L. O.: El Niño Driven Changes in Global Fire 2015/16, Frontiers in Earth Science, 8, https://doi.org/10.3389/feart.2020.00199, 2020.

Chadburn, S., Burke, E., Cox, P., Friedlingstein, P., Hugelius, G., and Westermann, S.: An observation-based constraint on permafrost loss as a function of global warming, Nature Climate Change, 7, 340–344, https://doi.org/10.1038/nclimate3262, 2017.

Clark, D. B., Mercado, L. M., Sitch, S., Jones, C. D., Gedney, N., Best, M. J., Pryor, M., Rooney, G. G., Essery, R. L. H., Blyth, E., Boucher, O., Harding, R. J., Huntingford, C., and Cox, P. M.: The Joint UK Land Environment Simulator (JULES), model description - Part 2: Carbon fluxes and vegetation dynamics, GEOSCIENTIFIC MODEL DEVELOPMENT, 4, 701–722, https://doi.org/10.5194/gmd-4-701-2011, 2011.

Collins, M., Knutti, R., Arblaster, J., Dufresne, J.-L., Fichefet, T., Friedlingstein, P., Gao, X., Gutowski, W., Johns, T., Krinner, G., Shongwe, M., Tebaldi, C., Weaver, A., and Wehner, M.: Long-term Climate Change: Projections, Commitments and Irreversibility, in: Climate Change 2013: The Physical Science Basis. Contribution of Working Group I to the Fifth Assessment Report of the Intergovernmental Panel on Climate Change, edited by Stocker, T., Qin, D., Plattner, G.-K., Tignor, M., Allen, S., Boschung, J., Nauels, A., Xia, Y., Bex, V., and Midgley, P., book section 12, p. 1029–1136, Cambridge University Press, Cambridge, United Kingdom and New York, NY, USA, https://doi.org/10.1017/CBO9781107415324.024, 2013.

https://doi.org/10.5194/egusphere-2023-2932
Preprint. Discussion started: 26 February 2024

Collins, W., Bellouin, N., Doutriaux-Boucher, M., Gedney, N., Halloran, P., Hinton, T., Hughes, J., Jones, C., Joshi, M., Liddicoat, S., Martin, G., O'Connor, F., Rae, J., Senior, C., Sitch, S., Totterdell, I., Wiltshire, A., and Woodward, S.: Development and evaluation of an Earth System model, HADGEM2, Geoscientific Model Development, 4, 1051–1075, https://doi.org/10.5194/gmd-4-1051-2011, 2011.

Cox, P. M.: Description of the TRIFFID dynamic global vegetation model, Tech. rep., https://digital.nmla.metoffice.gov.uk/IO_cc8f146a-d524-4243-88fc-e3a3bcd782e7/, 2001.

Drijfhout, S., Bathiany, S., Beaulieu, C., Brovkin, V., Claussen, M., Huntingford, C., Scheffer, M., Sgubin, G., and Swingedouw, D.: Catalogue of abrupt shifts in Intergovernmental Panel on Climate Change climate models, PROCEEDINGS OF THE NATIONAL ACADEMY OF SCIENCES OF THE UNITED STATES OF AMERICA, 112, E5777–E5786, https://doi.org/10.1073/pnas.1511451112, 2015.

Dvorak, M., Armour, K., Frierson, D., Proistosescu, C., Baker, M., and Smith, C.: Estimating the timing of geophysical commitment to 1.5 and 2.0° C of global warming, Nature Climate Change, 12, 547–552, 2022.

Eyring, V., Bony, S., Meehl, G. A., Senior, C. A., Stevens, B., Stouffer, R. J., and Taylor, K. E.: Overview of the Coupled Model Intercomparison Project Phase 6 (CMIP6) experimental design and organization, Geoscientific Model Development, 9, 1937–1958, https://doi.org/10.5194/gmd-9-1937-2016, 2016.

Forster, P., Storelvmo, T., Armour, K., Collins, W., Dufresne, J. L., Frame, D., Lunt, D. J., Mauritsen, T., Palmer, M. D., Watanabe, M., Wild, M., and Zhang, H.: The Earth's Energy Budget, Climate Feedbacks, and Climate Sensitivity, in: Climate Change 2021: The Physical Science Basis. Contribution of Working Group I to the Sixth Assessment Report of the Intergovernmental Panel on Climate Change, edited by Masson-Delmotte, V., Zhai, P., Pirani, A., Connors, S. L., Péan, C., Berger, S., Caud, N., Chen, Y., Goldfarb, L., Gomis, M. I., Huang, M., Leitzell, K., Lonnoy, E., Matthews, J. B. R., Maycock, T. K., Waterfield, T., Yelekçi, O., Yu, R., and Zhou, B., Cambridge University Press, https://www.ipcc.ch/report/ar6/wg1/downloads/report/IPCC_AR6_WGI_Chapter_07.pdf, 2021.

Forster, P. M., Smith, C. J., Walsh, T., Lamb, W. F., Lamboll, R., Hauser, M., Ribes, A., Rosen, D., Gillett, N., Palmer, M. D., Rogelj, J., von Schuckmann, K., Seneviratne, S. I., Trewin, B., Zhang, X., Allen, M., Andrew, R., Birt, A., Borger, A., Boyer, T., Broersma, J. A., Cheng, L., Dentener, F., Friedlingstein, P., Gutiérrez, J. M., Gütschow, J., Hall, B., Ishii, M., Jenkins, S., Lan, X., Lee, J.-Y., Morice, C., Kadow, C., Kennedy, J., Killick, R., Minx, J. C., Naik, V., Peters, G. P., Pirani, A., Pongratz, J., Schleussner, C.-F., Szopa, S., Thorne, P., Rohde, R., Rojas Corradi, M., Schumacher, D., Vose, R., Zickfeld, K., Masson-Delmotte, V., and Zhai, P.: Indicators of Global Climate Change 2022: annual update of large-scale indicators of the state of the climate system and human influence, Earth System Science Data, 15, 2295–2327, https://doi.org/10.5194/essd-15-2295-2023, 2023.

Frieler, K., Lange, S., Piontek, F., Reyer, C. P. O., Schewe, J., Warszawski, L., Zhao, F., Chini, L., Denvil, S., Emanuel, K., Geiger, T., Halladay, K., Hurtt, G., Mengel, M., Murakami, D., Ostberg, S., Popp, A., Riva, R., Stevanovic, M., Suzuki, T., Volkholz, J., Burke, E., Ciais, P., Ebi, K., Eddy, T. D., Elliott, J., Galbraith, E., Gosling, S. N., Hattermann, F., Hickler, T., Hinkel, J., Hof, C., Huber, V., Jägermeyr, J., Krysanova, V., Marcé, R., Müller Schmied, H., Mouratiadou, I., Pierson, D., Tittensor, D. P., Vautard, R., van Vliet, M., Biber, M. F., Betts, R. A., Bodirsky, B. L., Deryng, D., Frolking, S., Jones, C. D., Lotze, H. K., Lotze-Campen, H., Sahajpal, R., Thonicke, K., Tian, H., and Yamagata, Y.: Assessing the impacts of 1.5°C global warming – simulation protocol of the Inter-Sectoral Impact Model Intercomparison Project (ISIMIP2b), Geoscientific Model Development, 10, 4321–4345, https://doi.org/10.5194/gmd-10-4321-2017, 2017.

Frieler, K., Volkholz, J., Lange, S., Schewe, J., Mengel, M., Rivas López, M. d. R., Otto, C., Reyer, C. P., Karger, D. N., Malle, J. T., et al.: Scenario set-up and forcing data for impact model evaluation and impact attribution within the third round of the Inter-Sectoral Model Intercomparison Project (ISIMIP3a), EGUsphere, pp. 1–83, 2023.

https://doi.org/10.5194/egusphere-2023-2932
Preprint. Discussion started: 26 February 2024

Goodwin, P., Leduc, M., Partanen, A.-I., Matthews, H. D., and Rogers, A.: A computationally efficient method for probabilistic local warming projections constrained by history matching and pattern scaling, demonstrated by WASP–LGRTC-1.0, Geoscientific Model Development, 13, 5389–5399, https://doi.org/10.5194/gmd-13-5389-2020, 2020.

Herger, N., Sanderson, B. M., and Knutti, R.: .: Improved pattern scaling approaches for the use in climate impact studies, Geophysical Research Letters, 42, 3486–3494, https://doi.org/3486–3494, doi:10.1002/2015GL063569, 2015.

Huntingford, C. and Cox, P.: An analogue model to derive additional climate change scenarios from existing GCM simulations, CLIMATE DYNAMICS, 16, 575–586, https://doi.org/10.1007/s003820000067, 2000.

Huntingford, C., Booth, B. B. B., Sitch, S., Gedney, N., Lowe, J. A., Liddicoat, S. K., Mercado, L. M., Best, M. J., Weedon, G. P., Fisher, R. A., Lomas, M. R., Good, P., Zelazowski, P., Everitt, A. C., Spessa, A. C., and Jones, C. D.: IMOGEN: an intermediate complexity model to evaluate terrestrial impacts of a changing climate, GEOSCIENTIFIC MODEL DEVELOPMENT, 3, 679–687, https://doi.org/10.5194/gmd-3-679-2010, 2010.

IPCC: Climate Change 2021: The Physical Science Basis. Contribution of Working Group I to the Sixth Assessment Report of the Intergovernmental Panel on Climate Change, Cambridge University Press, Cambridge, UK and New York, NY, USA, https://doi.org/10.1017/9781009157896, 2021.

IPCC: Climate Change 2022: Mitigation of Climate Change. Contribution of Working Group III to the Sixth Assessment Report of the Intergovernmental Panel on Climate Change, Cambridge University Press, Cambridge, UK and New York, NY, USA, https://doi.org/10.1017/9781009157926, 2022.

James, R., Washington, R., Schleussner, C.-F., Rogelj, J., and Conway, D.: Characterizing half-a-degree difference: a review of methods for identifying regional climate responses to global warming targets, WIREs Climate Change, 8, e457, https://doi.org/https://doi.org/10.1002/wcc.457, 2017.

Jones, C. D., Hughes, J. K., Bellouin, N., Hardiman, S. C., Jones, G. S., Knight, J., Liddicoat, S., O'Connor, F. M., Andres, R. J., Bell, C., Boo, K.-O., Bozzo, A., Butchart, N., Cadule, P., Corbin, K. D., Doutriaux-Boucher, M., Friedlingstein, P., Gornall, J., Gray, L., Halloran, P. R., Hurtt, G., Ingram, W. J., Lamarque, J.-F., Law, R. M., Meinshausen, M., Osprey, S., Palin, E. J., Parsons Chini, L., Raddatz, T., Sanderson, M. G., Sellar, A. A., Schurer, A., Valdes, P., Wood, N., Woodward, S., Yoshioka, M., and Zerroukat, M.: The HadGEM2-ES implementation of CMIP5 centennial simulations, Geoscientific Model Development, 4, 543–570, https://doi.org/10.5194/gmd-4-543-2011, 2011.

Jones, C. D., Ziehn, T., Anand, J., Bastos, A., Burke, E., Canadell, J. G., Cardoso, M., Ernst, Y., Jain, A. K., Jeong, S., Keller, E. D., Kondo, M., Lauerwald, R., Lin, T.-S., Murray-Tortarolo, G., Nabuurs, G.-J., O'Sullivan, M., Poulter, B., Qin, X., von Randow, C., Sanches, M., Schepaschenko, D., Shvidenko, A., Smallman, T. L., Tian, H., Villalobos, Y., Wang, X., and Yun, J.: RECCAP2 Future Component: Consistency and Potential for Regional Assessment to Constrain Global Projections, AGU Advances, 4, e2023AV001 024, https://doi.org/https://doi.org/10.1029/2023AV001024, e2023AV001024 2023AV001024, 2023.

King, A. D., Lane, T. P., Henley, B. J., and Brown, J. R.: Global and regional impacts differ between transient and equilibrium warmer worlds, Nature Climate Change, 10, 42–47, 2020.

Leach, N. J., Jenkins, S., Nicholls, Z., Smith, C. J., Lynch, J., Cain, M., Walsh, T., Wu, B., Tsutsui, J., and Allen, M. R.: FaIRv2.0.0: A generalized impulse response model for climate uncertainty and future scenario exploration, Geoscientific Model Development, 14, 3007–3036, https://doi.org/10.5194/gmd-14-3007-2021, 2021.

Lee, J.-Y., Marotzke, J., Bala, G., Cao, L., Corti, S., Dunne, J., Engelbrecht, F., Fischer, E., Fyfe, J., Jones, C., Maycock, A., Mutemi, J., Ndiaye, O., Panickal, S., and Zhou, T.: Future Global Climate: Scenario-Based Projections and Near-Term Information, in: Climate Change

https://doi.org/10.5194/egusphere-2023-2932
Preprint. Discussion started: 26 February 2024

2021: The Physical Science Basis. Contribution of Working Group I to the Sixth Assessment Report of the Intergovernmental Panel on Climate Change, edited by Masson-Delmotte, V., Zhai, P., Pirani, A., Connors, S. L., Péan, C., Berger, S., Caud, N., Chen, Y., Goldfarb, L., Gomis, M. I., Huang, M., Leitzell, K., Lonnoy, E., Matthews, J. B. R., Maycock, T. K., Waterfield, T., Yelekçi, O., Yu, R., and Zhou, B., book section 4, Cambridge University Press, Cambridge, UK and New York, NY, USA, https://doi.org/10.1017/9781009157896.006, 2021.

Mathison, C., Burke, E., Hartley, A. J., Kelley, D. I., Burton, C., Robertson, E., Gedney, N., Williams, K., Wiltshire, A., Ellis, R. J., et al.: Description and Evaluation of the JULES-ES setup for ISIMIP2b, EGUsphere, 2022, 1–24, 2022.

McKay, D. I. A., Staal, A., Abrams, J. F., Winkelmann, R., Sakschewski, B., Loriani, S., Fetzer, I., Cornell, S. E., Rockström, J., and Lenton, T. M.: Exceeding 1.5°C global warming could trigger multiple climate tipping points, Science, 377, eabn7950, 2022.

Mercado, L. M., Bellouin, N., Sitch, S., Boucher, O., Huntingford, C., Wild, M., and Cox, P. M.: Impact of changes in diffuse radiation on the global land carbon sink, NATURE, 458, 1014–U87, https://doi.org/10.1038/nature07949, 2009.

Mitchell, T. D.: Pattern scaling: an examination of the accuracy of the technique for describing future climates, Climatic change, 60, 217–242, 2003.

Nath, S., Lejeune, Q., Beusch, L., Seneviratne, S. I., and Schleussner, C.-F.: MESMER-M: an Earth system model emulator for spatially resolved monthly temperature, Earth System Dynamics, 13, 851–877, https://doi.org/10.5194/esd-13-851-2022, 2022.

Nicholls, Z., Meinshausen, M., Lewis, J., Corradi, M. R., Dorheim, K., Gasser, T., Gieseke, R., Hope, A. P., Leach, N. J., McBride, L. A., Quilcaille, Y., Rogelj, J., Salawitch, R. J., Samset, B. H., Sandstad, M., Shiklomanov, A., Skeie, R. B., Smith, C. J., Smith, S. J., Su, X., Tsutsui, J., Vega-Westhoff, B., and Woodard, D. L.: Reduced Complexity Model Intercomparison Project Phase 2: Synthesizing Earth System Knowledge for Probabilistic Climate Projections, Earth's Future, 9, e2020EF001 900, https://doi.org/https://doi.org/10.1029/2020EF001900, e2020EF001900 2020EF001900, 2021.

Nicholls, Z. R. J., Meinshausen, M., Lewis, J., Gieseke, R., Dommenget, D., Dorheim, K., Fan, C.-S., Fuglestvedt, J. S., Gasser, T., Golüke, U., Goodwin, P., Hartin, C., Hope, A. P., Kriegler, E., Leach, N. J., Marchegiani, D., McBride, L. A., Quilcaille, Y., Rogelj, J., Salawitch, R. J., Samset, B. H., Sandstad, M., Shiklomanov, A. N., Skeie, R. B., Smith, C. J., Smith, S., Tanaka, K., Tsutsui, J., and Xie, Z.: Reduced Complexity Model Intercomparison Project Phase 1: introduction and evaluation of global-mean temperature response, Geoscientific Model Development, 13, 5175–5190, https://doi.org/10.5194/gmd-13-5175-2020, 2020.

Pugh, T. A. M., Jones, C. D., Huntingford, C., Burton, C., Arneth, A., Brovkin, V., Ciais, P., Lomas, M., Robertson, E., Piao, S. L., and Sitch, S.: A Large Committed Long-Term Sink of Carbon due to Vegetation Dynamics, Earth's Future, 6, 1413–1432, https://doi.org/https://doi.org/10.1029/2018EF000935, 2018.

Pörtner, H. O., Roberts, D. C., Tignor, M., Poloczanska, E. S., Mintenbeck, K., Alegría, A., Craig, M., Langsdorf, S., Löschke, S., Möller, V., Okem, A., and Rama, B., eds.: Full report, p. In Press, Cambridge University Press, Cambridge, UK, in Press, 2022.

Quilcaille, Y., Gudmundsson, L., Beusch, L., Hauser, M., and Seneviratne, S. I.: Showcasing MESMER-X: Spatially Resolved Emulation of Annual Maximum Temperatures of Earth System Models, Geophysical Research Letters, 49, e2022GL099 012, https://doi.org/https://doi.org/10.1029/2022GL099012, e2022GL099012 2022GL099012, 2022.

Riahi, K., Schaeffer, R., Arango, J., Calvin, K., Guivarch, C., Hasegawa, T., Jiang, K., Kriegler, E., Matthews, R., Peters, G. P., Rao, A., Robertson, S., Sebbit, A. M., Steinberger, J., Tavoni, M., and Vuuren, D. P. V.: Mitigation pathways compatible with long-term goals., in: IPCC, 2022: Climate Change 2022: Mitigation of Climate Change. Contribution of Working Group III to the Sixth Assessment Report of the Intergovernmental Panel on Climate Change, edited by Shukla, P. R., Skea, J., Slade, R., Khourdajie, A. A., van Diemen, R.,

https://doi.org/10.5194/egusphere-2023-2932
Preprint. Discussion started: 26 February 2024

McCollum, D., Pathak, M., Some, S., Vyas, P., Fradera, R., Belkacemi, M., Hasija, A., Lisboa, G., Luz, S., and Malley, J., Cambridge University Press, https://doi.org/10.1017/9781009157926.005, 2022.

Richters, O., Bertram, C., Kriegler, E., Al Khourdajie, A., Cui, R., Edmonds, J., Hackstock, P., Holland, D., Hurst, I., Kikstra, J., Lewis, J., Liadze, I., Meinshausen, M., Min, J., Nicholls, Z., Piontek, F., Sauer, I., Sferra, F., Sanchez Juanino, P., van Ruijven, B., Weigmann, P., Yu, S., Zhao, A., and Zwerling, M.: NGFS Climate Scenarios Data Set, https://doi.org/10.5281/zenodo.7198430, This work was made possible by grants from Bloomberg Philanthropies and ClimateWorks Foundation., 2022.

Rogelj, J., Shindell, D., Jiang, K., Fifita, S., Forster, P., Ginzburg, V., Handa, C., Kheshgi, H., Kobayashi, S., Kriegler, E., Mundaca, L., Séférian, R., and Vilariño, M. V.: Mitigation Pathways Compatible with 1.5°C in the Context of Sustainable Development, in: Global Warming of 1.5°C: An IPCC Special Report on the impacts of global warming of 1.5°C above pre-industrial levels and related global greenhouse gas emission pathways, in the context of strengthening the global response to the threat of climate change, sustainable development, and efforts to eradicate poverty, edited by Masson-Delmotte, V., Zhai, P., Pörtner, H.-O., Roberts, D., Skea, J., Shukla, P. R., Pirani, A., Moufouma-Okia, W., Péan, C., Pidcock, R., Connors, S., Matthews, J. B. R., Chen, Y., Zhou, X., Gomis, M. I., Lonnoy, E., Maycock, T., Tignor, M., and Waterfield, T., World Meteorological Organization, Geneva, Switzerland, https://www.ipcc.ch/sr15/, 2018.

Sellar, A. A., Jones, C. G., Mulcahy, J. P., Tang, Y., Yool, A., Wiltshire, A., O'connor, F. M., Stringer, M., Hill, R., Palmieri, J., et al.: UKESM1: Description and evaluation of the UK Earth System Model, Journal of Advances in Modeling Earth Systems, 11, 4513–4558, 2019.

Smith, C.: FaIR v1.6.2 calibrated and constrained parameter set, https://doi.org/10.5281/zenodo.6601980, 2022.

Smith, C. J., Forster, P. M., Allen, M., Leach, N., Millar, R. J., Passerello, G. A., and Regayre, L. A.: FAIR v1.3: a simple emissions-based impulse response and carbon cycle model, Geoscientific Model Development, 11, 2273–2297, https://doi.org/10.5194/gmd-11-2273-2018, 2018.

Smith, C. J., Nicholls, Z. R. J., Armour, K., Collins, W., Forster, P., Meinshausen, M., Palmer, M. D., and Watanabe, M.: The Earth's Energy Budget, Climate Feedbacks, and Climate Sensitivity Supplementary Material, in: Climate Change 2021: The Physical Science Basis. Contribution of Working Group I to the Sixth Assessment Report of the Intergovernmental Panel on Climate Change, edited by Masson-Delmotte, V., Zhai, P., Pirani, A., Connors, S. L., Péan, C., Berger, S., Caud, N., Chen, Y., Goldfarb, L., Gomis, M. I., Huang, M., Leitzell, K., Lonnoy, E., Matthews, J. B. R., Maycock, T. K., Waterfield, T., Yelekçi, O., Yu, R., and Zhou, B., Cambridge University Press, https://www.ipcc.ch/report/ar6/wg1/downloads/report/IPCC_AR6_WGI_Chapter_07_Supplementary_Material.pdf, 2021.

Stanhill, G. and Cohen, S.: Global dimming: a review of the evidence for a widespread and significant reduction in global radiation with discussion of its probable causes and possible agricultural consequences, Agricultural and Forest Meteorology, 107, 255–278, https://doi.org/https://doi.org/10.1016/S0168-1923(00)00241-0, 2001.

Taylor, K. E., Stouffer, R. J., and Meehl, G. A.: An Overview of CMIP5 and the Experiment Design, Bulletin of the American Meteorological Society, 93, 485–498, https://doi.org/https://doi.org/10.1175/BAMS-D-11-00094.1, 2012.

Tebaldi, C. and Arblaster, J. M.: Pattern scaling: Its strengths and limitations, and an update on the latest model simulations, Climatic Change, 122, 459–471, 2014.

Tebaldi, C. and Knutti, R.: Evaluating the accuracy of climate change pattern emulation for low warming targets, Environmental Research Letters, 13, 055 006, https://doi.org/10.1088/1748-9326/aabef2, 2018.

Tebaldi, C., Snyder, A., and Dorheim, K.: STITCHES: creating new scenarios of climate model output by stitching together pieces of existing simulations, Earth System Dynamics, 13, 1557–1609, https://doi.org/10.5194/esd-13-1557-2022, 2022.

https://doi.org/10.5194/egusphere-2023-2932
Preprint. Discussion started: 26 February 2024

van Vuuren, D. P., Lowe, J., Stehfest, E., Gohar, L., Hof, A. F., Hope, C., Warren, R., Meinshausen, M., and Plattner, G.-K.: How well do integrated assessment models simulate climate change?, Climatic Change, 104, 255–285, https://doi.org/10.1007/s10584-009-9764-2, 2011.

Varney, R. M., Chadburn, S. E., Burke, E. J., Jones, S., Wiltshire, A. J., and Cox, P. M.: Simulated responses of soil carbon to climate change in CMIP6 Earth system models: the role of false priming, Biogeosciences, 20, 3767–3790, 2023.

Wang Z, Zhang M, W. L. Q. W.: A comprehensive research on the global all-sky surface solar radiation and its driving factors during 1980–2019., Atmos Research, 265, https://doi.org/https://doi.org/10.1016/j.atmosres.2021.105870.

Warszawski, L., Friend, A., Ostberg, S., Frieler, K., Lucht, W., Schaphoff, S., Beerling, D., Cadule, P., Ciais, P., Clark, D. B., Kahana, R., Ito, A., Keribin, R., Kleidon, A., Lomas, M., Nishina, K., Pavlick, R., Rademacher, T. T., Buechner, M., Piontek, F., Schewe, J., Serdeczny, O., and Schellnhuber, H. J.: A multi-model analysis of risk of ecosystem shifts under climate change, Environmental Research Letters, 8, 044 018, http://stacks.iop.org/1748-9326/8/i=4/a=044018, 2013.

Warszawski, L., Frieler, K., Huber, V., Piontek, F., Serdeczny, O., and Schewe, J.: The Inter-Sectoral Impact Model Intercomparison Project (ISI-MIP): Project framework, Proceedings of the National Academy of Sciences, 111, 3228–3232, https://doi.org/10.1073/pnas.1312330110, 2014.

Wells, C. D., Jackson, L. S., Maycock, A. C., and Forster, P. M.: Understanding pattern scaling errors across a range of emissions pathways, Earth System Dynamics, 14, 817–834, https://doi.org/10.5194/esd-14-817-2023, 2023.

Williams, K. and Clark, D.: Hadley Centre Technical Note 96 Disaggregation of daily data in JULES, Tech. rep., Met Office, 2014.

Wiltshire, A. J., Burke, E. J., Chadburn, S. E., Jones, C. D., Cox, P. M., Davies-Barnard, T., Friedlingstein, P., Harper, A. B., Liddicoat, S., Sitch, S., et al.: JULES-CN: a coupled terrestrial carbon–nitrogen scheme (JULES vn5. 1), Geoscientific Model Development, 14, 2161–2186, 2021.

Zelazowski, P., Huntingford, C., Mercado, L. M., and Schaller, N.: Climate pattern-scaling set for an ensemble of 22 GCMs – adding uncertainty to the IMOGEN version 2.0 impact system, Geoscientific Model Development, 11, 541–560, https://doi.org/10.5194/gmd-11-541-2018, 2018.